American Mineralogist, Volume 94, pages 64–73, 2009

Dehydration dynamics of barrerite: An in situ synchrotron XRPD study

Silvia Ori, Edoardo Mazzucato, and Giovanna Vezzalini*

Dipartimento di Scienze della Terra, Largo S. Eufemia, 19, I-41100 Modena, Italy

Abstract

The thermally induced structural modifications of the natural zeolite barrerite [$Na_{16}Al_{16}Si_{56}O_{144}\cdot 52H_2O$, a = 13.6239(4) Å, b = 18.2033(5) Å, c = 17.8317(7) Å, V = 4422.3(3) Å^3, space group *Amma*, framework type STI] were studied in a temperature-resolved X-ray powder diffraction experiment, using synchrotron radiation, in the temperature range 339–973 K. In the initial stage of heating, up to 508 K, barrerite Phase A (space group *Amma*) is stable, the unit-cell volume decreases by about 4% and a water release of about 66% is observed. Between 521 and 598 K, a phase transition to the collapsed so-called barrerite Phase B (space group *Amma*) is observed. During the transition, the rotation of the 4^25^4 secondary building units causes a large decrease in cell volume and deformation of the channel system. Phase B, at 611 K, shows the statistical breaking of T-O-T bridges in the 4-rings and the migration of the involved tetrahedral atoms to new "face-sharing" tetrahedra, with a consequent reduction of the free volume of the channels parallel to [100]. The new structure is stable up to 741 K and the total volume decrease is about 16%. A new phase appears from 754 K with cell parameters similar to those reported for the highly deformed barrerite Phase D and is stable up to 910 K, which is the temperature at which the total volume decrease is 22.5%. The material does not undergo amorphization up to the highest temperature investigated.

Keywords: Zeolite, barrerite, dehydration, X-ray powder diffraction, synchrotron radiation, crystal structure

Introduction

The high-temperature stability of zeolites and their behavior during the dehydration process are widely studied topics because of the diverse industrial applications of these phases as molecular sieves, sorbents, and catalysts. A knowledge of the structural modifications induced by dehydration and the definition of the stability fields of these materials is of prime importance to assure their persistence and effectiveness in technological applications. The structural changes induced by dehydration in natural and synthetic microporous phases have been reviewed recently by Bish and Carey (2001), Alberti and Martucci (2005), and Cruciani (2006). In these papers, the authors were looking for some rationalization of the factors governing zeolite thermal stability and their structural changes. Besides structural features like framework topology, framework density (FD) (Baerlocher et al. 2001), Si/Al ratio, (Si,Al) ordering in the tetrahedra, and ionic potential of charge-compensating cations, several external factors were considered as possible controls on the thermal behavior of zeolites. Among these, the dehydration temperature, the presence of water vapor, the effect of vacuum, the crystal size, the heating rate, and, in general, the dehydration kinetics followed during the dehydration experiments were considered. Specifically, the structural effects obtained during a stepwise ex-situ experiment (thus in a status near to equilibrium) or with continuous in-situ heating (thus far from equilibrium) have been demonstrated to be different for the zeolite stellerite (Arletti et al. 2006). Cruciani (2006) introduced an empirical Stability index (SI), based on the collapse/breakdown temperature—determined by X-ray studies—together with the maximum volume contraction and the presence of phase transformations, thus defining five different groups of SI values from 1 to 5. However, the author found only a general, rather than consistent, correlation between this factor and the Si/Al ratio or the ionic potential of extraframework cations. In contrast, no relationship was observed between SI and FD. The conclusion of Cruciani's paper is that, "the picture we have of the factors controlling the response to heating is still quite fragmentary."

The classification of zeolite thermal behavior of Alberti and Vezzalini (1984), also adopted by Bish and Carey (2001), divides zeolites into three categories. (1) Zeolites in which reversible dehydration is accompanied by rearrangement of extraframework cations without marked changes in the framework structure and in the cell volume. (2) Zeolites in which reversible dehydration is accompanied by a strong distortion of the framework and a large decrease of cell volume. (3) Zeolites in which dehydration is accompanied by topological changes as a consequence of T-O-T bridge breaking.

In this last case, the reversibility of the dehydration, which is considered one of the most remarkable properties of zeolites, is not always completely fulfilled, at least in the short term. This is the case for zeolites whose framework is built from differently connected chains of 4^25^4 secondary building units (SBUs) (units formed by two 4-rings and four 5-rings of tetrahedra): stilbite (Slaughter 1970; Mortier 1983; Cruciani et al. 1997), barrerite (Galli and Alberti 1975b; Alberti and Vezzalini 1978; Alberti et al. 1983), stellerite (Galli and Alberti 1975a; Alberti et al. 1978; Arletti et al. 2006), heulandite (Merkle and Slaughter 1968; Alberti 1972, 1973; Alberti and Vezzalini 1983; Alberti et al.

* E-mail: giovanna@unimore.it

1985), clinoptilolite (Armbruster and Gunter 1991; Armbruster 1993), and brewsterite (Alberti et al. 1999, 2001; Ståhl and Hanson 1999; Sacerdoti et al. 2000), where the dehydration process results in transformation into one or more new phases (Alberti and Vezzalini 1984).

Barrerite (ideal formula: $Na_{16}Al_{16}Si_{56}O_{144}\cdot 52H_2O$; space group *Amma*, alternative setting of the space group *Cmcm*) (Galli and Alberti 1975b) shares with stilbite (ideal formula: $Na_2Ca_8Al_{18}Si_{54}O_{144}\cdot 60H_2O$; space group *C*2/*m*) (Slaughter 1970; Mortier 1983) and stellerite (ideal formula: $Ca_8Al_{16}Si_{56}O_{144}\cdot 58H_2O$; space group *Fmmm*) (Galli and Alberti 1975a; Miller and Taylor 1985) the STI framework type (space group *Fmmm*) (code defined in Baerlocher et al. 2001), but the different content and distribution of extraframework cations impose different real symmetry and different thermal behavior in the three phases (Alberti et al. 1978; Arletti et al. 2006; Alberti and Vezzalini 1978; Cruciani et al. 1997).

The STI type framework can be described by the joining of the 4^25^4 SBUs to form chains parallel to the *c* axis. Such chains are laterally connected by six oxygen bridges to form layers parallel to (010). Another two oxygen bridges link the layers to each other, thus forming a three dimensional net. Two systems of channels result in the structure, a 10-ring channel running parallel to the *a* axis (Fig. 1) and an 8-ring channel running along the *c* axis.

The different space groups observed in stilbite, stellerite, and barrerite are determined by the number and distribution of cations on different extraframework sites. In stellerite, the eight Ca cations are located in one set of equivalent extraframework positions (labeled Ca site) (Galli and Alberti 1975a), nearly at the center of the 10-ring channel at an *mm*2 position (Wyckoff notation 4*c*). They are completely surrounded by water molecules without any contact with the O atoms of the framework. In stilbite eight Ca cations occupy the same position (labeled Ca site) (Galli 1971) as in stellerite, whereas two Na cations are localized in a new site (labeled Na). The electrostatic repulsive forces between the extraframework cations in the Na and Ca sites are strong enough to push the calcium out of one of the two mirror planes and to force the framework to rotate, lowering the symmetry to *C*2/*m*. In barrerite, 16 monovalent cations are distributed not only in C1 and C1p sites corresponding to the Ca site of stilbite and stellerite, and in C2p, broadly corresponding to the Na site of stilbite, but also in two other sites, C2 and C3 (Galli and Alberti 1975b). The charge repulsion between the cations at C1, C1p, and C2p is here counteracted by the presence of cations in C2, which push the cations in C1 and C1P in opposite directions, and consequently the orthorhombic symmetry is restored (see Fig. 3 in Galli and Alberti 1975a). The presence of cations in site C3 forces the framework to rotate around the screw diad parallel to *a*, leading to the real symmetry *Amma*. It should be pointed out that, in the Na-exchanged stellerite studied by Passaglia and Sacerdoti (1982), the *Fmmm* symmetry is exactly maintained for the whole framework, whereas it is retained for the extraframework cations only on a statistical basis.

The high-temperature structures of stellerite (Alberti et al. 1978) and barrerite (Alberti and Vezzalini 1978) were studied by conventional ex situ experiments, i.e., through single-crystal diffraction, performed at room temperature, on crystals previously

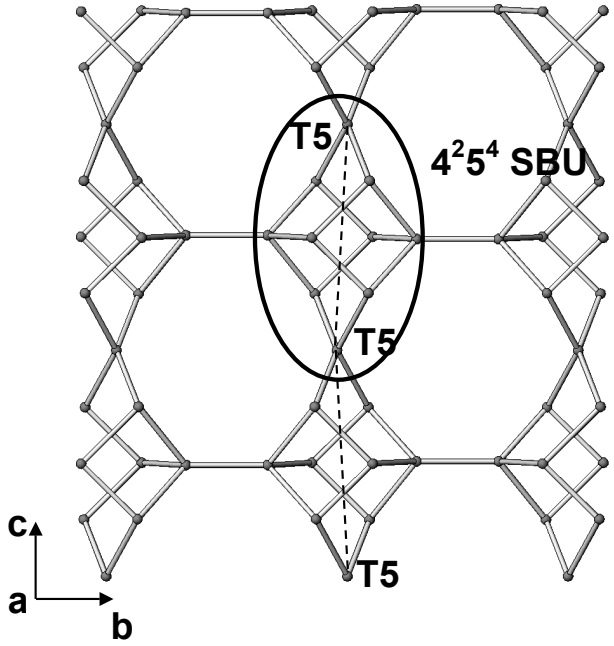

FIGURE 1. Projection along [100] of the STI type framework, showing the 10mR-channel system and the 4^25^4 SBUs chain.

dehydrated in vacuum, or in air, at selected temperatures. These studies showed that, in both zeolites, the collapsed so-called B phases (and the partially rehydrated Phase C of barrerite, obtained by cooling barrerite Phase B to room temperature) have space group *Amma*, undergo rotation of the SBUs, with a consequent pronounced zigzag of the SBU chains, and present the statistical breaking of the same T-O-T bridge in the 4-ring. This process is accompanied by the migration of the tetrahedral cations involved to new, partially occupied, tetrahedral sites (with three O atoms in common with the previously occupied ones) in a "face-sharing" relationship with the original tetrahedra. Whereas in barrerite the vertices of the new tetrahedra may or may not be shared by tetrahedra of adjacent SBUs, in stellerite they are always unshared and occupied by hydroxyl groups, generating an interrupted framework characterized by a wider freedom of movement in the channels. This structural feature results in a different behavior upon rehydration: after one year in air, the unit cell of stellerite reassumes the volume of Phase A, while that of barrerite is similar to that of the partially rehydrated Phase C. This latter phase, obtained by maintaining barrerite B at room temperature for a short time, is always characterized by an interrupted framework, but its unit-cell volume is 4% larger with respect to Phase B as a consequence of the partial re-hydration. Moreover, heating barrerite to higher temperature resulted in a new stable phase, called barrerite D, more contracted than barrerite B, but, owing to the poor quality of the data, its structure was not determined (Alberti and Vezzalini 1978). Recently Sacerdoti (2007) solved the structure of barrerite D by single-crystal X-ray diffraction. In this phase a unit-cell volume contraction of 18.9% is observed and a lowering of the symmetry from space group *Amma* to $A2_1ma$ is reported. This structure differs from the original one and does not show an interrupted framework.

Some specimens of cation-exchanged stilbite (NH_4 and Na/

NH_4), dehydrated up to 603 K and studied by single-crystal X-ray diffraction, showed the same weakness point in the framework and hence the same T-O-T bond was broken (Pearce et al. 1980; Mortier 1983).

The dehydration dynamics of stilbite was studied using in situ synchrotron X-ray powder diffraction (XRPD) (Cruciani et al. 1997). In their work the authors showed that a contracted Phase B is formed at about 402 K, but in this case the T-O-T bridge breaking mainly involves different tetrahedra of the 4-ring compared to those observed in barrerite and stellerite. Recently Arletti et al. (2006), studying the dehydration dynamics of stellerite—also using in situ synchrotron X-ray powder diffraction (XRPD)—noted the influence of the dehydration kinetics on T-O-T bridge breaking. In this case, in fact, the framework breaking occurs in the same T-O bond observed in the stilbite in situ study, and so differs from that observed in stellerite during the ex situ experiment. The authors conclude that the experimental conditions, inducing a different evolution of the extraframework species and thus a different influence on the framework deformation, play a primary role in the dehydration process of STI type zeolites.

Barrerite, the Na-term of the STI type zeolites, is a rare zeolite originally found near Capo Pula (Sardinia, Italy) by Passaglia and Pongiluppi (1974, 1975) and more recently recognized in the basaltic lavas of Kuiu and Kupreanof Islands (Alaska) (Di Renzo and Gabelica 1997; Sacerdoti et al. 1999). The genesis of this mineral was interpreted by Passaglia et al. (1978) as due to crystallization of stellerite, followed by Na-exchange with seawater.

The aims of this work are (1) to study the dehydration dynamics of barrerite by in situ synchrotron XRPD; (2) to compare the results with the data obtained by single-crystal ex situ experiments; and (3) to confirm the influence of kinetics on the structural modifications induced by the dehydration process in zeolites with STI-type framework.

Experimental methods

The barrerite sample used in this work is from Kuiu Island, Alaska (sample number 3 in Sacerdoti et al. 1999). Its chemical composition is

$$Na_{7.90}K_{3.18}Mg_{0.28}Ca_{1.98}Al_{16.64}Si_{55.36}O_{144}\cdot 50.8H_2O.$$

The unit-cell parameters determined at room temperature (RT) are a = 13.6239(4) Å, b = 18.2033(5) Å, c = 17.8317(7) Å, V = 4422.3(3) Å^3.

Data collection

The temperature-resolved XRPD experiment was performed at the Italian GILDA beam line, operating at the European Synchrotron Radiation Facilities (ESRF, Grenoble, France). The powdered sample of barrerite was carefully packed inside a 0.5 mm capillary open at both ends. Data was acquired in parallel Debye-Scherrer geometry, with an LaB_6 refined wavelength of 0.95337 Å; the rotating capillary sample was heated in situ by means of a hot air stream, with a heating rate of 5.1 K/min, from 339 K up to 973 K. The apparatus was calibrated with the thermal expansion of MgO (diffraction data collected in the same experimental conditions) for the whole temperature range. Moreover, the decomposition temperatures of kaolinite and calcite were also tested. The powder diffraction patterns were continuously collected, during the whole heating process, on the 4 mm slit-delimited slice of a translating imaging plate detector (Norby 1997; Meneghini et al. 2001), located at a sample-to-detector distance of 204.2 mm. A total of 49 powder patterns were extracted by integrating temperature slices of about 13 K width and separation between subsequent integration intervals of about 10 K (Fig. 2). Each powder pattern was measured for about 2.5 min.

The first pattern on the imaging plate was collected at 339 K, instead of room temperature, due to a technical problem. To investigate the complete thermal behavior of barrerite a powder pattern at room temperature, on a different powder sample, was subsequently measured on a Philips PANalytical X'PERT Pro, at the Centro Grandi Strumenti of the University of Modena and Reggio Emilia. The barrerite powder sample was packed inside a 0.5 mm capillary open at both ends and the data were acquired with Cu$K\alpha$ radiation. The powder diffraction pattern was collected in the 2θ range 5–120; soller slit was 0.02 rad, diverging slits ¼° of 2θ, and antiscatter X'Celerator slit 5 mm.

Structure refinement

The GSAS package (Larson and Von Dreele 2000) with the EXPGUI (Toby 2001) interface was used for Rietveld profile fitting. The structure refinement was carried out on 19 patterns of the 49 available, 12 of barrerite Phase A, covering the temperature range 339–482 K, and 7 of barrerite Phase B, covering the temperature range 611–689 K. In the temperature range 521–598 K, owing to the coexistence of both barrerite Phases A and B, only unit-cell parameters were calculated in a two phase refinement using the structures refined for Phase A at 482 K and for Phase B at 637 K, respectively (see Fig. 2 and Table 1). Above 741 K the growth of new peaks (Fig. 2) suggested the possibility of a further phase transition to barrerite Phase D and only the unit-cell parameters were extracted up to 910 K. Above this temperature the quality of the data were not good enough to allow a satisfactory refinement of the unit-cell parameters.

The extracted Bragg peak profiles were modeled by a pseudo-Voigt function with 2 refined coefficients (one Gaussian and one Lorenzian term, Gw and Ly in GSAS terminology) and a 0.02% cut-off of the peak intensity. Anisotropic peak broadening, modeled with GSAS parameters ptec and stec, was negligible. The background curve was fitted with a refined 20-coefficient Chebyshev polynomial. Soft-constraints were applied to the T-O distances and gradually released after the initial stages of refinement. The thermal displacement parameters were constrained in the following way: the same value for all tetrahedral atoms, a second value for all framework O atoms, and a third for extraframework cations and water molecules, since the charge-compensating cations were represented mainly by sodium.

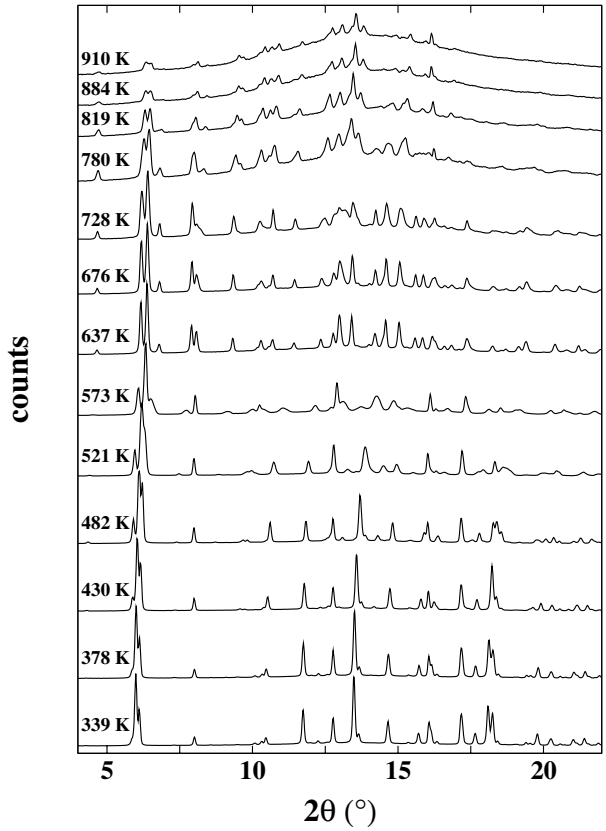

Figure 2. Selected integrated powder XRD patterns of barrerite as a function of temperature in the 2θ range 4–22°.

TABLE 1. Unit-cell parameters of barrerite as a function of temperature

T (K)	*a* (Å)	*b* (Å)	*c* (Å)	*V* (Å^3)
298_A	13.6239(4)	18.2033(5)	17.8317(7)	4422.3(3)
339_A	13.6336(3)	18.2056(4)	17.8445(4)	4429.1(2)
352_A	13.6331(2)	18.1960(3)	17.8378(3)	4424.96(7)
365_A	13.6338(2)	18.1864(3)	17.8303(3)	4421.04(7)
378_A	13.6354(2)	18.1743(3)	17.8224(3)	4416.64(7)
391_A	13.6379(2)	18.1587(3)	17.8108(3)	4410.78(8)
404_A	13.6409(2)	18.1373(3)	17.7933(3)	4402.23(8)
417_A	13.6456(2)	18.1088(3)	17.7664(3)	4390.20(8)
430_A	13.6520(2)	18.0723(3)	17.7312(3)	4374.68(8)
443_A	13.6580(2)	18.0345(2)	17.6927(3)	4358.0(1)
456_A	13.6654(2)	17.9921(3)	17.6542(3)	4340.6(1)
469_A	13.6702(2)	17.9424(4)	17.6147(4)	4320.5(1)
482_A	13.6744(2)	17.8937(4)	17.5723(4)	4299.7(1)
495_A	13.6782(4)	17.8433(6)	17.5217(7)	4276.4(3)
508_A	13.6793(4)	17.7735(6)	17.4558(6)	4244.0(2)
521_A	13.678(1)	17.684(1)	17.345(2)	4188(1)
521_B	13.676(2)	17.666(2)	17.335(1)	4033(6)
534_A	13.663(1)	17.549(2)	17.199(2)	4124.0(9)
534_B	13.667(3)	17.446(3)	17.128(4)	4084(2)
547_A	13.637(2)	17.439(2)	17.078(3)	4061(1)
547_B	13.638(3)	17.374(4)	16.984(4)	4024(2)
559_A	13.621(2)	17.374(3)	16.978(3)	4018(1)
559_B	13.625(3)	17.319(3)	16.838(3)	3794(1)
572_A	13.603(3)	17.313(3)	16.823(4)	3962(1)
572_B	13.609(2)	17.256(2)	16.581(2)	3894(1)
585_A	13.580(3)	17.286(4)	16.549(4)	3885(1)
585_B	13.580(1)	17.195(1)	16.318(2)	3810.3(7)
598_A	13.567(3)	17.241(4)	16.390(4)	3834(1)
598_B	13.5708(9)	17.170(1)	16.197(1)	3774.1(5)
611_B	13.5625(5)	17.1593(7)	16.1416(6)	3756.5(3)
624_B	13.5559(4)	17.1537(5)	16.1093(5)	3745.9(2)
637_B	13.5502(4)	17.1487(6)	16.0919(5)	3739.3(2)
650_B	13.5453(5)	17.1437(7)	16.0829(6)	3734.7(3)
663_B	13.5383(6)	17.1392(8)	16.0787(7)	3730.8(4)
676_B	13.5324(7)	17.135(1)	16.0757(8)	3727.6(4)
689_B	13.5217(9)	17.129(1)	16.074(1)	3722.9(5)
702_B	13.5212(9)	17.1255(9)	16.0679(9)	3720.6(3)
715_B	13.510(1)	17.140(1)	16.086(1)	3724.7(4)
728_B	13.443(2)	17.092(2)	16.052(2)	3688.2(8)
741_B	13.381(2)	17.048(2)	16.049(2)	3661.3(9)
754_B	13.451(2)	17.071(2)	16.040(2)	3683.3(9)
754_D	13.186(3)	16.935(3)	16.010(3)	3575.1(9)
767_D	13.145(2)	16.912(3)	15.994(3)	3555.7(8)
780_D	13.127(2)	16.906(3)	15.986(3)	3547.5(9)
793_D	13.104(3)	16.889(3)	15.971(3)	3535(1)
806_D	13.078(3)	16.872(3)	15.950(3)	3519(1)
819_D	13.044(3)	16.840(3)	15.908(3)	3494(1)
832_D	13.012(3)	16.802(3)	15.863(4)	3468(1)
845_D	12.987(3)	16.776(3)	15.847(3)	3452(1)
858_D	12.967(3)	16.750(3)	15.825(3)	3437(1)
871_D	12.946(3)	16.727(4)	15.812(3)	3424(1)
884_D	12.947(4)	16.732(4)	15.807(4)	3424(1)
897_D	12.947(4)	16.727(4)	15.812(5)	3425(2)
910_D	12.944(7)	16.734(7)	15.838(8)	3431(2)

Note: The A, B, and D suffixes refer to barrerite Phases A, B, and D, respectively.

In the barrerite sample, impurities of quartz were detected and the amount was refined to about 2 wt%. Because only a few quartz peaks were evident in the patterns, its lattice parameters showed a strong correlation with the zero shift values. Given the impossibility of refining the lattice parameters in a satisfactory way, the thermal expansion of quartz (Ackermann and Sorrell 1974) was imposed.

Two scale factors, one for quartz and one for barrerite, the zero-shift, and the unit-cell parameters of barrerite were allowed to vary for all refinement cycles. In the final cycles, the refined structural parameters for each data histogram were as follows: fractional coordinates for all atoms, occupancy factors for extraframework cations, water oxygen, and partially occupied framework atoms and thermal isotropic displacement factors, as explained above. Occupancy factors and isotropic thermal displacement factors were varied in alternate cycles. Scattering factors for neutral atoms are those listed by Cromer and Waber (1974).

At room temperature, the structure of barrerite Phase A (sample number 3 in Sacerdoti et al. 1999) was used as a starting model for the framework atoms, whereas the extraframework sites were located by difference Fourier maps. The Rietveld refinement of the powder patterns converged successfully up to 482 K. Above this temperature, the difficulty in the structure refinement and the growth of new peaks above 508 K suggested the possibility of a phase transition. As shown in Figure 2, the stabilization of the patterns was evident above 611 K, and the pattern at 637 K was consistent with the structure of barrerite Phase B of Alberti and Vezzalini (1978). The framework structural model reported by these authors was thus assumed for all the patterns where Phase B was observed. The extraframework sites were located by a combination of difference Fourier maps and least squares refinements. The site labeling reported by Sacerdoti et al. (1999) was used for Phase A. As regards Phase B, to maintain the same orientation of the SBUs during the dehydration process, a unit-cell origin change was imposed with respect to the data reported by Alberti and Vezzalini (1978). The new origin is –1/2, –1/2, and +1/2 along *x*, *y*, and *z* unit-cell axes, respectively. As a consequence, the atoms labeled with the suffix P in Alberti and Vezzalini (1978) are here labeled without the suffix P (for example the T1P atom of Alberti and Vezzalini corresponds to the T1 atom of this study).

Above 741 K, the growth of new peaks (Fig. 2) suggested the possibility of the further phase transition to barrerite Phase D, a phase initially identified by Alberti and Vezzalini (1978) and whose structure was recently solved by Sacerdoti (2007). However, the co-existence of both Phases B and D, the low peak to background ratio, the broadening of the diffraction peaks, and the presence of a large amount of an amorphous phase, did not allow a satisfactory structure refinement (see Fig. 2) and only the unit-cell parameters of Phase D were extracted up to 910 K (Table 1).

The refinement details for patterns at 339, 482, and 637 K are reported in Table 2, the refined atomic coordinates, occupancy factors, and thermal parameters for the structures at the same temperatures are reported in Table 3 and the bond distances are reported in Table 4. Figure 3 shows the observed and calculated diffraction patterns and final difference curve from Rietveld refinements of barrerite A at 339 and 482 K (Figs. 3a–3b) and barrerite B at 637 K (Fig. 3c). For the sample at T_{amb}, only unit-cell parameters are given because, as reported above, the powder sample is different from that used for the temperature-resolved experiment and, as reported by Sacerdoti et al. (1999), the barrerite samples from Kuiu Island, Alaska, are inhomogeneous both in chemical composition and in the structural features of the extraframework content.

RESULTS

The only phase present between room temperature and 508 K is barrerite Phase A (space group *Amma*) and the unit-cell parameter variations in this *T* range are 0.4, –2.3, and –2.1%, for *a*, *b*, and *c*, respectively, with a volume contraction of 4% (Fig. 4 and Table 1). In the temperature range 521–598 K, a phase transition to the so-called Phase B (Alberti and Vezzalini 1978) occurs and the volume further contracts by about 10%. In this *T* range, owing to the coexistence of both A and B Phases, only the unit-cell parameters were derived: Phase A up to 508 K, Phase B from 611 K onward, and both phases between 508 and 611 K (Fig. 4 and Table 1). Only barrerite Phase B is stable between 611 and 689 K. In this temperature range, stabilization of the cell parameters is observed and the total decrease in unit-cell volume at 689 K is about 16%. Above this temperature, the difficulty in the structure refinement and the growth, above 741 K, of new diffraction peaks in the powder patterns (Fig. 2)

TABLE 2. Experimental and refinement parameters for barrerite at 339, 482, and 637 K

	BAR-A 339 K	BAR-A 482 K	BAR-B 637 K
a (Å)	13.6336(3)	13.6744(2)	13.5502(4)
b (Å)	18.2056(4)	17.8937(4)	17.1487(6)
c (Å)	17.8445(4)	17.5723(4)	16.0919(5)
Cell volume (Å^3)	4429.1(2)	4299.7(1)	3739.3(2)
Space group	*Amma* (*Cmcm*)	*Amma* (*Cmcm*)	*Amma* (*Cmcm*)
R_p (%)	3.67	4.11	3.09
R_{wp} (%)	5.03	6.89	4.12
$R_{F^{**}2}$ (%)	7.60	12.97	10.76
No. of variables	122	105	110
No. of observations	5049	5050	4635
No. of reflections	1430	1385	841

TABLE 3. Fractional coordinates, thermal parameters, and site occupancy factors (Occ.) of barrerite Phase A at 339 and 482 K and of barrerite Phase B at 637 K

	BAR-A 339 K					BAR-A 482 K				
	x/a	*y/b*	*z/c*	Occ.	U_{iso}	*x/a*	*y/b*	*z/c*	Occ.	U_{iso}
T1	0.1354(5)	0.3066(4)	0.1264(4)	1.00	0.046(6)	0.1362(4)	0.2920(3)	0.1230(3)	1.00	0.049(1)
T1P	0.1340(5)	0.3092(4)	0.3748(4)	1.00	0.046(6)	0.1335(4)	0.3248(3)	0.3696(3)	1.00	0.049(1)
T3	0.0512(3)	0.4112(2)	0.2459(5)	1.00	0.046(6)	0.0472(4)	0.4095(3)	0.2298(3)	1.00	0.049(1)
T4	0.1400(3)	0.1845(2)	0.2490(5)	1.00	0.046(6)	0.1403(4)	0.1867(3)	0.2643(3)	1.00	0.049(1)
T5	0.00	0.2388(5)	0.00	1.00	0.046(6)	0.00	0.2156(4)	0.00	1.00	0.049(1)
O1	0.0722(8)	0.2921(5)	0.0486(5)	1.00	0.054(1)	0.0723(6)	0.2733(5)	0.0462(5)	1.00	0.065(1)
O1P	0.0716(8)	0.3181(5)	0.4537(5)	1.00	0.054(1)	0.0690(8)	0.3396(5)	0.4477(6)	1.00	0.065(1)
O3	0.122(1)	0.2308(6)	0.1719(7)	1.00	0.054(1)	0.122(1)	0.2316(6)	0.1876(5)	1.00	0.065(1)
O3P	0.126(1)	0.2363(6)	0.3229(6)	1.00	0.054(1)	0.132(1)	0.2419(5)	0.3351(6)	1.00	0.065(1)
O4	0.102(1)	0.3825(6)	0.1686(6)	1.00	0.054(1)	0.1083(8)	0.3735(5)	0.1577(6)	1.00	0.065(1)
O4P	0.103(1)	0.3753(6)	0.3195(6)	1.00	0.054(1)	0.1013(8)	0.3865(6)	0.3092(5)	1.00	0.065(1)
O7	0.25	0.310(1)	0.097(1)	1.00	0.054(1)	0.25	0.3081(9)	0.0924(9)	1.00	0.065(1)
O7P	0.25	0.3226(9)	0.396(1)	1.00	0.054(1)	0.25	0.3422(8)	0.3884(9)	1.00	0.065(1)
O8	0.0657(5)	0.1138(4)	0.246(1)	1.00	0.054(1)	0.0685(6)	0.1178(5)	0.2719(7)	1.00	0.065(1)
O9	0.0525(9)	0.50	0.240(1)	1.00	0.054(1)	0.056(1)	0.50	0.2173(9)	1.00	0.065(1)
O10	0.25	0.1495(6)	0.254(2)	1.00	0.054(1)	0.25	0.1453(8)	0.2642(9)	1.00	0.065(1)
C1	0.25	0.00	0.045(9)	0.30(20)	0.071(3)	0.25	0.00	−0.032(2)	0.44(2)	0.123(5)
C1P	0.25	0.00	0.463(2)	0.66(3)	0.071(3)	0.25	0.00	0.450(6)	0.21(2)	0.123(5)
C2	0.048(2)	0.064(2)	0.004(2)	0.27(1)	0.071(3)	0.074(2)	−0.010(2)	0.088(2)	0.21(1)	0.123(5)
C2P	0.100(1)	0.078(1)	0.431(1)	0.43(1)	0.071(3)	0.083(2)	0.105(1)	0.468(1)	0.39(1)	0.123(5)
C3	0.193(3)	0.00	0.289(2)	0.32(3)	0.071(3)	0.209(4)	0.00	0.233(4)	0.24(2)	0.123(5)
W1P	0.152(2)	0.155(2)	0.445(2)	0.40(1)	0.071(3)					
W2	0.25	0.124(1)	0.065(2)	0.73(2)	0.071(3)	0.25	0.126(3)	0.095(2)	0.35(2)	0.123(5)
W2P	0.25	0.129(3)	0.447(3)	0.36(3)	0.071(3)	0.25	0.139(3)	0.432(4)	0.27(2)	0.123(5)
W3	0.164(3)	0.00	0.164(3)	0.39(2)	0.071(3)					
W3P	0.25	0.00	0.336(5)	0.40(5)	0.071(3)					
W4	0.211(9)	0.00	0.056(5)	0.40(10)	0.071(3)					
W4P	0.071(5)	0.00	0.401(5)	0.25(3)	0.071(3)	0.291(5)	0.00	0.310(4)	0.32(2)	0.123(5)
W5	0.152(4)	0.50	0.061(3)	0.31(2)	0.071(3)	0.094(1)	0.50	0.074(1)	0.80(2)	0.123(5)
W6	0.046(6)	0.50	−0.035(6)	0.58(2)	0.071(3)					
W6P	0.402(2)	0.50	0.426(2)	0.21(3)	0.071(3)					
W8	0.25	0.50	0.096(2)	0.62(4)	0.071(3)	0.25	0.50	0.098(4)	0.35(2)	0.123(5)
W8P	0.25	0.50	0.380(3)	0.52(3)	0.071(3)	0.25	0.50	0.340(2)	0.93(2)	0.123(5)
CA*						0.00	0.039(4)	0.00	0.15(1)	0.123(5)

suggested the possibility of a further phase transition to a new phase, with unit-cell parameters similar to those reported for the highly deformed barrerite D (Alberti and Vezzalini 1978; Sacerdoti 2007). This phase is stable up to 910 K. At this temperature a total volume decrease of 22.5% is observed. Up to the highest temperature investigated the material does not undergo amorphization (Fig. 2).

HT-induced framework modifications

The structural features of the framework of barrerite Phase A remain substantially unchanged up to 508 K, although, as visible in Figure 5 for the structure at 482 K, a slight deformation of the 10-ring channels is observed. The T5-T5 and T1-T1P distances, corresponding to the 4^25^4 SBU dimensions, are quite constant in this initial temperature range (Fig. 6a). By contrast, a rotation of the units around their center of gravity imposes a variation of the T5-T5-T5 angle of about 10° (Fig. 6b).

The framework of barrerite Phase B is characterized, as already highlighted in the single-crystal study (Alberti and Vezzalini 1978), by a more accentuated rotation of the SBUs, which causes a zigzag shape of the SBU chains along the *c* axis, a cell-volume contraction, and a further deformation of both the channels parallel to the *a* and *c* axes (Fig. 5). As a result of the unit rotation, above 611 K, the statistical breaking of the oxygen bridge T1-O3-T4 of the 4-ring is observed. Together with this effect a migration of the two involved tetrahedral cations from T1 and T4 to the new partially occupied "face-sharing" tetrahedra, called T1D and T4D was observed (Fig. 5c; Tables 3 and 4). The new tetrahedra T1D and T4D share three O atoms with the previously occupied one, whereas the new vertex (OD) is at an appropriate bond distance from the two new tetrahedral cations of adjacent units. This framework modification corresponds to that found by Alberti and Vezzalini (1978) in the so-called barrerite Phase B. In this collapsed phase two kinds of building units are present as a result of the statistical bridge breaking: one is the original one, i.e., a 4^25^4 unit, the other one is formed by two 5-membered rings and two very irregular 7-membered rings (Fig. 5c). The percentage of broken bridges is unchanged with temperature as shown in Table 3 and in Figures 7a and 7b, where the occupancies of T1, T1D, T4, and T4D are reported. Because the occupancy factors of T1D, T4D, and OD are nearly equal, the new "face-sharing" tetrahedra of adjacent SBUs always have to be linked and the OD site always has to be occupied by an O atom, thus forming a different but not interrupted framework. In any case, the channels parallel to [100] are partially occluded, passing the delimiting ring from 10 to 9 or 8 tetrahedra (see Fig. 5c), whereas the channels parallel to [001] are not influenced by the presence of the new tetrahedra.

Extraframework sites

In the structure of barrerite at room temperature, Sacerdoti et al. (1999) recognized 14 sites occupied by water molecules and five occupied by charge compensating cations, although the bond distances between extraframework cation sites and framework O atoms did not allow a precise location of different cations in the five sites. In the structural refinements reported here, almost all the bond distances between extraframework sites and framework O atoms are larger than 3.2 Å. This fact,

TABLE 3.—CONTINUED

	BAR-B 637 K										
	x/a	*y/b*	*z/c*	Occ.	U_{iso}		*x/a*	*y/b*	*z/c*	Occ.	U_{iso}
T1	0.6480(9)	0.7823(7)	–0.1152(8)	0.44(1)	0.074(2)	O7P	0.75	0.8968(10)	–0.3788(10)	1.00	0.097(2)
T1P	0.6384(6)	0.8604(4)	–0.3621(5)	1.00	0.074(2)	O8	0.5746(8)	0.6184(7)	–0.3069(10)	1.00	0.097(2)
T3	0.5391(6)	0.9095(3)	–0.1990(5)	1.00	0.074(2)	O9	0.5393(20)	1.00	–0.1810(10)	1.00	0.097(2)
T4	0.6484(8)	0.6926(6)	–0.2885(8)	0.52(1)	0.074(2)	O10	0.75	0.6425(8)	–0.3022(10)	1.00	0.097(2)
T5	0.50	0.8228(6)	–0.50	1.00	0.074(2)	OD	0.6553(20)	0.6483(10)	–0.4520(10)	0.50(2)	0.077(10)
T1D	0.6330(6)	0.8179(6)	–0.0437(9)	0.56(1)	0.074(2)	C1	0.549(9)	0.50	–0.507(4)	0.29(10)	0.051(6)
T4D	0.6540(9)	0.6730(6)	–0.3550(10)	0.48(1)	0.074(2)	C2	0.50	0.525(7)	–0.50	0.22(10)	0.051(6)
O1	0.5666(8)	0.7382(5)	–0.0552(5)	1.00	0.097(2)	C3	0.539(2)	0.50	0.006(2)	0.43(1)	0.051(6)
O1P	0.5597(9)	0.8802(5)	–0.4367(6)	1.00	0.097(2)	C4	0.75	1.00	–0.281(2)	0.53(2)	0.051(6)
O3	0.6720(20)	0.7377(10)	–0.2022(10)	0.48(1)	0.097(2)	C5	0.634(9)	0.573(6)	–0.142(7)	0.08(1)	0.051(6)
O3P	0.6286(9)	0.7657(5)	–0.3516(9)	1.00	0.097(2)	W1	0.75	1.00	–0.143(6)	0.23(2)	0.051(6)
O4	0.5974(10)	0.8685(7)	–0.1241(8)	1.00	0.097(2)	W2	0.630(4)	0.50	–0.206(5)	0.24(2)	0.051(6)
O4P	0.6140(9)	0.9060(8)	–0.2758(7)	1.00	0.097(2)	W3	0.622(5)	0.530(5)	–0.487(4)	0.14(1)	0.051(6)
O7	0.75	0.8020(10)	–0.0635(10)	1.00	0.097(2)	W4	0.675(3)	0.50	–0.102(3)	0.33(2)	0.051(6)

the variability of the occupancy factors of extraframework sites at the various temperatures, the variability of the bond distances with the framework, and the possible rearrangement of water molecules and cations on the extraframework sites, made it difficult to understand the evolution of the cation-water molecule system. Therefore, for each temperature, the number of water molecules was calculated by subtracting from the total number of electrons—obtained from the refined occupancy factors of all the extraframework sites—those corresponding to the cations, assumed as constant during the whole dehydration process (see Fig. 8). For the sake of clarity, the labels of the extraframework sites of barrerite Phase A and Phase B in Tables 3 and 4 were maintained. In Figure 8, the number of water molecules calculated in this way is plotted as a function of temperature. In general, one can see that about two thirds of water is lost before the transition to barrerite Phase B and that almost all the rest is removed before the transition to Phase D. However, this further water loss does not influence the cell parameters, which remain almost constant. Phase D can be assumed as completely anhydrous as already reported by Sacerdoti (2007). The evolution of water molecules discussed above is in good agreement with the thermogravimetric analysis.

In Tables 3 and 4, the coordinates and bond distances for barrerite Phase A at 339 and 482 K (the highest *T* at which the structure refinement of Phase A was reliable), and for barrerite Phase B at 637 K are reported. At 482 K we can observe that W1P, W3, W3P, W4, W6, and W6P water molecules are already lost and a total of about 16 water molecules are retained in the structure. As regards the extraframework cation sites, the same positions as the structure at 339 K are found, while the occupancy factors are rather different from the original ones; moreover a new site (labeled CA*) is also found.

Five cation and four water molecule sites in the Phase B structure were located. These positions are the same as those reported by Alberti and Vezzalini (1978)—with the exception of W2—but different from those of Phase A (Tables 3 and 4). At 637 K, a water content corresponding to about 7.5 water molecules is still retained.

DISCUSSION

Behavior of barrerite as a function of dehydration conditions

In the ex situ dehydration study of barrerite, performed on a single crystal (Alberti and Vezzalini 1978), Phase B was obtained by heating the sample for 16 h in air in the temperature range 473–653 K and immediately cooling it to room temperature. Hence it can be assumed that the dehydration kinetics was slow and that the system was near equilibrium. The same procedure was used to obtain Phase D, i.e., heating the sample above 673 K. In this work, on the contrary, a continuous fast heating rate, in air, was applied and so we can assume that conditions were far from equilibrium.

Comparing the thermal behavior of barrerite studied using different kinetics, we can observe some similarities and some differences. In particular, in both experiments a similar volume decrease is observed for Phases B and D. The framework breaking, observed in Phase B, involves the same T-O-T bridge with migration of both tetrahedral cations to new "face-sharing" tetrahedra and this occurs with the same frequency.

The framework deformation and the subsequent T-O-T bridge breaking, observed during the dehydration of all STI type zeolites, were interpreted by several authors (Alberti and Vezzalini 1978, 1984; Alberti et al. 1978; Arletti et al. 2006; Cruciani et al. 1997) as due to the strain induced by extraframework cations on the framework O atoms, to achieve energetically more favorable coordination during water release. This effect in barrerite is less evident as the extraframework cations are distributed on many sites, weakly bonded to framework O atoms, and the coordinated water molecules are released at higher temperatures.

Some significant differences can be singled out in the transition temperatures to both B and D Phases. In the temperature-resolved experiment the transitions from Phase A to Phase B, and from B to D occur above 508 K and above 741 K, respectively, while in the ex situ experiment the temperatures are 473 and 673 K, respectively. In our experiment the faster kinetics thus induce a delay in the process of phase transformation; in fact at 473 and 673 K we still observe Phase A and Phase B, respectively. Moreover, we find the same water content of Phase B as Alberti and Vezzalini (1978) (6.7 water molecules at 523 K) only at 650 K.

Comparison of dehydration mechanisms of STI type zeolites

Considering the dehydration mechanisms of the zeolites with STI type framework, studied in temperature-resolved experiments, some conclusions can be drawn. In the three zeolites the *a* parameter is essentially unchanged and the *c* parameter, along which the chain of $4^2 5^4$ SBUs runs, is characterized by the

TABLE 4. Interatomic distances of barrerite Phase A at 339 and 482 and of barrerite Phase B at 637 K

	BAR-A 339 K	BAR-A 482 K		BAR-A 339 K	BAR-A 482 K
T1-O1	1.654(6)	1.642(6)	T4-O3	1.633(6)	1.588(6)
T1-O3	1.612(6)	1.579(6)	T4-O3P	1.633(6)	1.592(6)
T1-O4	1.639(6)	1.626(6)	T4-O8	1.639(5)	1.582(6)
T1-O7	1.648(5)	1.671(6)	T4-O10	1.631(5)	1.674(5)
mean	1.638	1.630	mean	1.634	1.609
T1P-O1P	1.653(6)	1.653(6)	T5-O1	1.632(4)	1.645(5)
T1P-O3P	1.622(6)	1.602(6)	T5-O1	1.632(4)	1.645(5)
T1P-O4P	1.614(6)	1.593(6)	T5-O1P	1.645(5)	1.646(5)
T1P-O7P	1.644(5)	1.656(5)	T5-O1P	1.645(5)	1.646(5)
mean	1.633	1.626	mean	1.639	1.646
T3-O4	1.630(6)	1.649(6)			
T3-O4P	1.628(6)	1.632(6)			
T3-O8	1.663(5)	1.656(6)			
T3-O9	1.620(4)	1.638(5)			
mean	1.635	1.644			
C1-O7P		3.15(2)	C2P-O1	3.19(2)	2.57(3)
C1-C2x4	3.08(5)	3.21(4)	C2P-O1		3.05(2)
C1-W2x2	2.29(4)	3.18(5)	C2P-C1P	2.55(2)	2.98(3)
C1-W3x2	2.4(2)		C2P-C2P	2.83(4)	2.53(4)
C1-W4x2	0.6(1)		C2P-C3	3.17(4)	
C1-W6Px2	3.0(1)		C2P-W1P	1.59(3)	
C1-W8P	2.9(2)	2.25(3)	C2P-W2P	2.26(3)	2.45(3)
			C2P-W3P	3.01(5)	
C1P-C2Px4	2.55(2)	2.98(3)	C2P-W4P	1.57(4)	
C1P-C3x2	3.18(6)		C2P-W5	2.81(5)	2.65(2)
C1P-W1Px4	3.15(3)		C2P-W5		3.15(2)
C1P-W2Px2	2.37(6)	2.50(7)	C2P-W6	1.71(6)	
C1P-W4Px2	2.68(7)	2.5(1)	C2P-W6	3.07(8)	
C1P-W5x2	2.21(6)	3.05(7)			
C1P-W6x2	2.78(8)		C3-O8x2	2.82(3)	2.93(4)
C1P-W8	2.38(5)	2.6(1)	C3-O10x2	2.90(2)	2.72(2)
			C3-C1P	3.18(6)	
C2-O1P	2.36(3)		C3-C2x2		3.15(8)
C2-O1P	2.80(3)		C3-C2Px2	3.17(4)	
C2-C1	3.08(5)	3.21(4)	C3-C3	1.55(8)	1.1(1)
C2-C2	2.31(6)	0.4(2)	C3-W3	2.28(6)	
C2-C2	2.66(5)		C3-W3	2.97(6)	
C2-C2	1.30(5)		C3-W3P	1.14(6)	
C2-C3		3.15(8)	C3-W4P	2.60(9)	1.34(5)
C2-CA*		1.93(5)	C3-W4P		1.75(6)
C2-CA*		2.06(6)			
C2-W2	3.17(3)	3.18(8)	CA*O1Px2		2.54(7)
C2-W4	2.7(1)		CA*C2x2		1.93(5)
C2-W6P	1.94(4)		CA*C2x2		2.06(6)
C2-W6P	2.61(3)		CA*CA*		1.4(2)
W1P-C1P	3.15(3)		W4P-C1P	2.68(7)	2.5(1)
W1P-C2P	1.59(3)		W4P-C2Px2	1.57(4)	
W1P-W2P	1.42(3)		W4P-C3	2.60(9)	1.34(5)
			W4P-C3		1.75(6)
W2-C1	2.29(4)	3.18(5)	W4P-W4P		1.1(1)
W2-C2x2	3.17(3)	3.18(8)	W4P-W6	1.20(8)	
W2P-C1P	2.37(6)	2.50(7)	W5-C1P	2.21(6)	3.05(7)
W2P-C2Px2	2.26(3)	2.45(3)	W5-C2Px2	2.81(5)	3.15(2)
W2P-W1Px2	1.42(3)		W5-C2Px2		2.65(2)
			W5-W8	1.47(5)	2.17(2)
W3-C1	2.4(2)				
W3-C3	2.28(6)		W6-C1P	2.78(8)	
W3-C3	2.97(6)		W6-C2Px2	1.71(6)	
W3-W4	2.0(1)		W6-C2Px2	3.07(8)	
			W6-W4P	1.20(8)	
W3P-C1P	2.26(9)		W6-W6	1.8(2)	
W3P-C2Px4	3.01(5)				
W3P-C3x2	1.13(6)		W6P-C1	3.0(1)	
			W6P-C2x2	1.94(4)	
W4-C1	0.6(1)		W6P-C2x2	2.61(3)	
W4-C2x2	2.7(1)				
W4-W3	2.0(1)		W8-C1P	2.38(5)	2.6(1)
W4-W4	1.1(2)		W8-W5x2	1.47(5)	2.17(2)
			W8P-C1	2.9(2)	2.25(3)

TABLE 4.—CONTINUED

	BAR-B 637 K		BAR-B 637 K
T1-O1	1.649(7)	T4-O3	1.622(8)
T1-O3	1.628(8)	T4-O3P	1.637(7)
T1-O4	1.636(7)	T4-O8	1.644(7)
T1-O7	1.648(7)	T4-O10	1.637(7)
mean	1.640	mean	1.635
T1P-O1P	1.642(7)	T5-O1	1.642(5)
T1P-O3P	1.638(7)	T5-O1	1.642(5)
T1P-O4P	1.628(7)	T5-O1P	1.631(5)
T1P-O7P	1.658(7)	T5-O1P	1.631(5)
mean	1.642	mean	1.637
T3-O4	1.601(7)		
T3-O4P	1.600(7)		
T3-O8	1.617(7)		
T3-O9	1.580(5)		
mean	1.600		
T1D-O1	1.646(7)	T4D-O3P	1.629(7)
T1D-O4	1.632(7)	T4D-O8	1.623(8)
T1D-O7	1.640(7)	T4D-O10	1.638(7)
T1D-OD	1.613(8)	T4D-OD	1.618(8)
mean	1.633	mean	1.627
C1-O4x2	3.01(6)	OD-C1	3.06(7)
C1-O9	2.80(6)	OD-C2	3.08(9)
C1-ODx2	3.06(7)	OD-W3	2.15(8)
C1-C1	1.3(3)		
C1-C2x2	0.79(7)	W1-C4	2.23(8)
C1-W3x2	1.2(1)		
C1-W3x2	2.4(2)	W2-C5x2	1.6(1)
		W2-W4	1.78(8)
C2-O4x2	3.01(8)		
C2-O9x2	2.99(3)	W3-OD	2.15(8)
C2-ODx4	3.08(9)	W3-C1	1.2(1)
C2-C1x2	1.79(7)	W3-C1	2.4(2)
C2-C2	0.9(3)	W3-C2	1.67(7)
C2-W3x2	1.67(7)	W3-C2	1.9(1)
C2-W3x2	1.9(1)	W3-W3	1.0(2)
C3-O1Px2	2.27(2)		
C3-O1Px2	2.70(2)	W4-C3	2.53(5)
C3-C3	1.08(5)	W4-C5x2	1.5(1)
C3-C5x2	3.0(1)	W4-C5x2	2.9(1)
C3-W4	2.53(5)	W4-W2	1.78(8)
		W4-W4	2.03(8)
C4-O4Px4	2.45(1)		
C4-O7Px2	2.36(3)		
C4-W1	2.23(8)		
C5-O1P	3.0(1)		
C5-O3	3.0(1)		
C5-O8	2.9(1)		
C5-C3	3.0(1)		
C5-C5	3.2(2)		
C5-C5	2.5(2)		
C5-W2	1.6(1)		
C5-W4	1.5(1)		
C5-W4	2.9(1)		

largest decrease. In both stilbite and stellerite, the total unit-cell volume contraction is about 8%, while in barrerite the decrease is about 16%. In particular the largest *c* parameter variation is observed in barrerite, in correspondence with the largest T5-T5-T5 angle decrease.

The initial dehydration step in stilbite and stellerite is accompanied by a phase transition, with a symmetry change to space group *Amma*, and this new phase is called Phase B. Only in a second step does the dehydration induce the T-O-T bridge breaking. In a different way, barrerite Phase B is defined on the basis only of framework breaking, because the symmetry remains unchanged in the A and B phases.

Stilbite and stellerite Phases B develop at 423 K, are stable up to 723 and 773 K, respectively, and the T-O-T bridge breaking

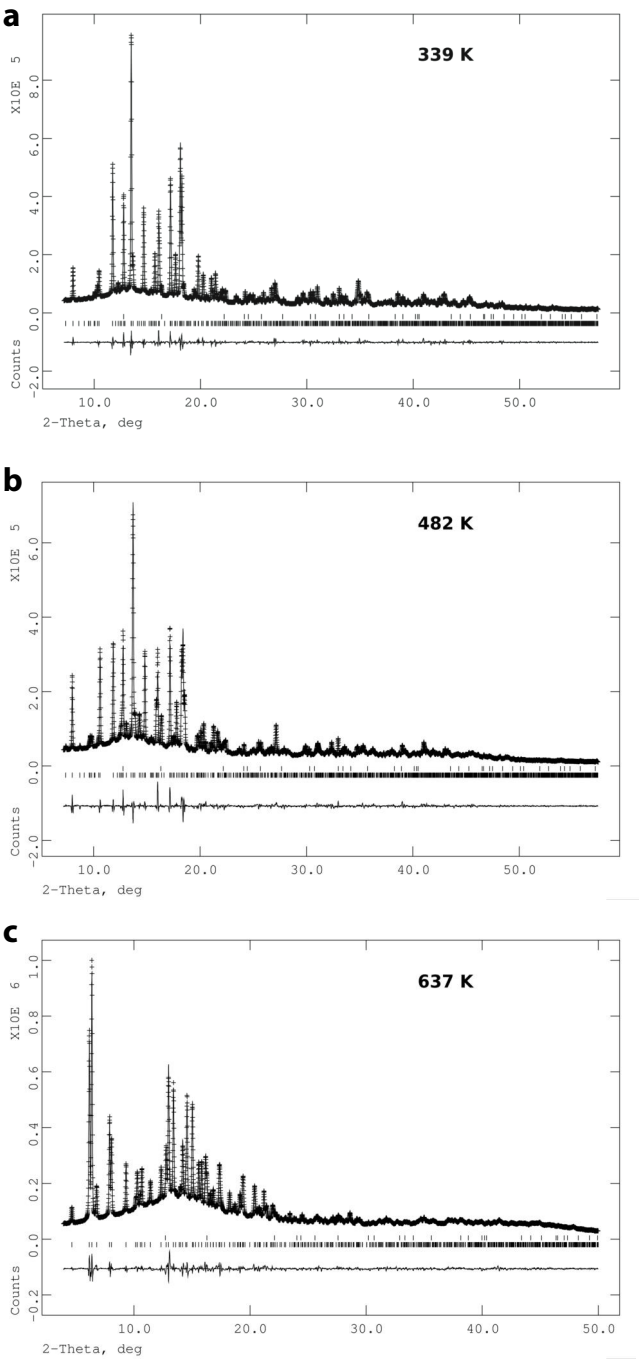

FIGURE 3. Observed (crossed line) and calculated (continuous line) diffraction patterns and final difference curve from Rietveld refinements of barrerite A at (**a**) 339 K and (**b**) 482 K and of barrerite B at (**c**) 637 K.

is observed above 523 K. Stellerite amorphization is observed above 773 K, while the stilbite in situ experiment was performed only up to 723 K and thus the amorphization effect was not seen. Barrerite B grows at 523 K and is the only phase stable up to 723 K. Above this temperature Phase D develops and no complete amorphization is observed up to 973 K. Therefore, we can assume that the *T*-range in which the framework breaking occurs is the same in all the STI type zeolites; however, barrerite, evolving into Phase D, is stable up to the highest temperatures. Cruciani (2006) introduced a new empirical parameter, called the stability index (SI) based on the breakdown temperature from X-ray diffraction studies, to quantify the thermal stability of zeolites. Following this method, we can assume a SI of 4 for barrerite, compared to a value of 3 for stilbite and stellerite.

The framework bridge breaking in stilbite and stellerite occurs in the same T-O bond and the migration of tetrahedral cations to the new "face-sharing" tetrahedra involves only one of the two tetrahedra engaged in the breaking. In barrerite, the breaking involves a different T-O-T bridge and both the tetrahedral cations move to the new tetrahedra, forming a new uninterrupted framework. The presence of the new T-O-T bridge, between adjacent SBUs of the same chain, contributes to the major framework deformation and unit-cell volume decrease. In particular, the T5-T5 distance, length of the $4^2 5^4$ SBU and dependent on its deformation, is 8.42 Å in Phase B of barrerite (Fig. 6a), as compared to 8.77 and 8.80 Å in that of stilbite and stellerite. The breaking frequency varies from 40 to 50% in the three zeolites.

In stilbite and stellerite Phase A only a few extraframework cation sites are found and the dehydration process induces a spreading of cations into more positions, while in barrerite the number of sites occupied by cations is large but remains the same in both Phases A and B. In stilbite and stellerite at 603 K, no more water is present in structure cavities, while in barrerite Phase B about 3.6 water molecules are still found at 689 K. The presence of this residual water could act as a catalyst, promoting the breaking of further bonds (Alberti and Vezzalini 1984, Donnay et al. 1959), favoring the transition to Phase D (Sacerdoti 2007), and contributing to the larger stability field of barrerite compared to stilbite and stellerite.

Thus, it can be concluded that, in barrerite, the dehydration kinetics do not play a primary role in governing the position of T-O-T bridge breaking as observed, by contrast, in stellerite (Arletti et al. 2006). In this phase, the dehydration method induces a different evolution of the extraframework species with a consequent influence on the deformation and breaking of the framework. However, in the two experiments on stellerite a

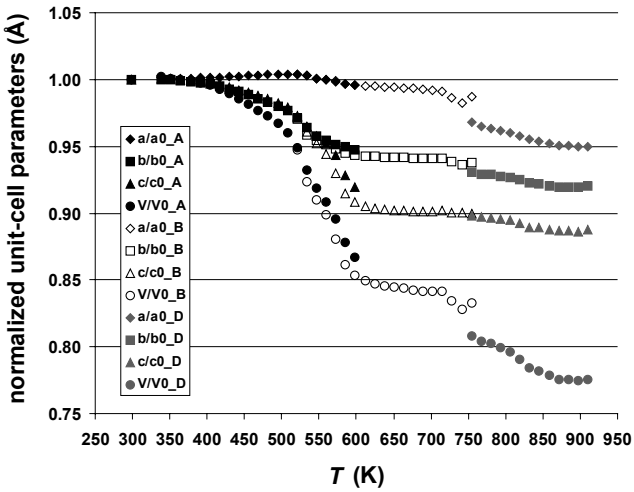

FIGURE 4. Plot of normalized unit-cell parameters and unit-cell volume of barrerite vs. temperature. A, B, and D labels refer to barrerite Phases A, B, and D, respectively. The errors are smaller than the symbols.

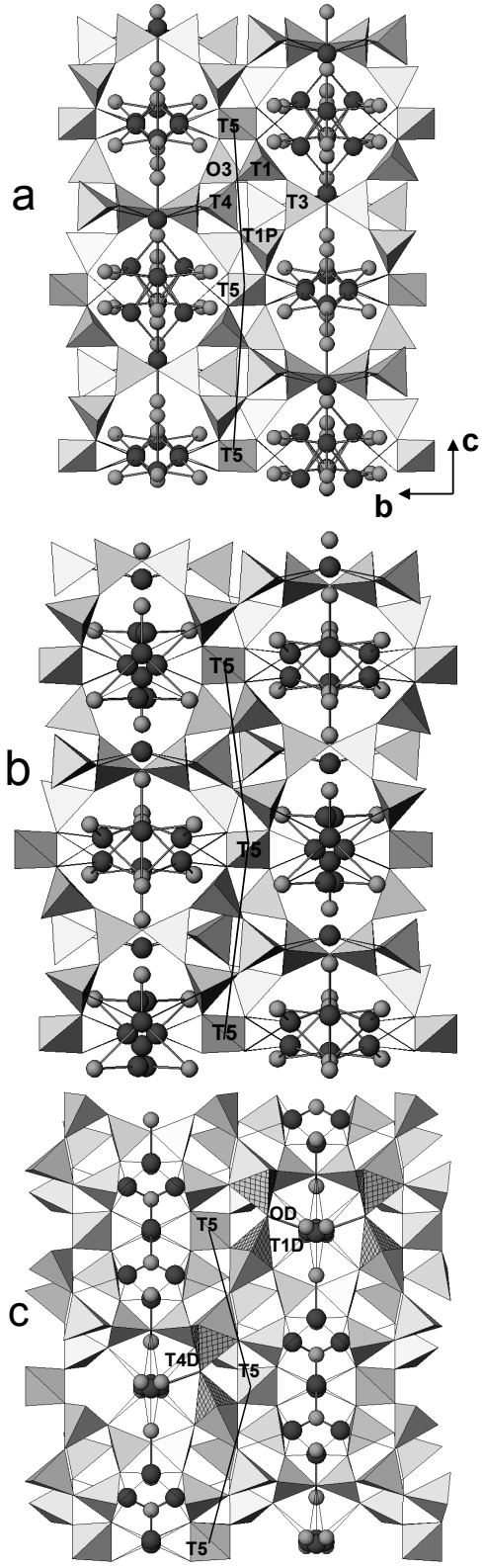

FIGURE 5. Projection along [100] of the refined structure of barrerite Phase A at (**a**) 339 K and (**b**) 482 K, and barrerite Phase B at (**c**) 637 K. Na atoms = large dark gray spheres; water molecules = small light gray spheres; Na-water (thick line) and Na-$O_{framework}$ (thin line) bond distances <3.2 Å are drawn. In **c**, some possible configurations of the Phase B framework are shown; the new "face sharing" tetrahedra are drawn with crossed lines.

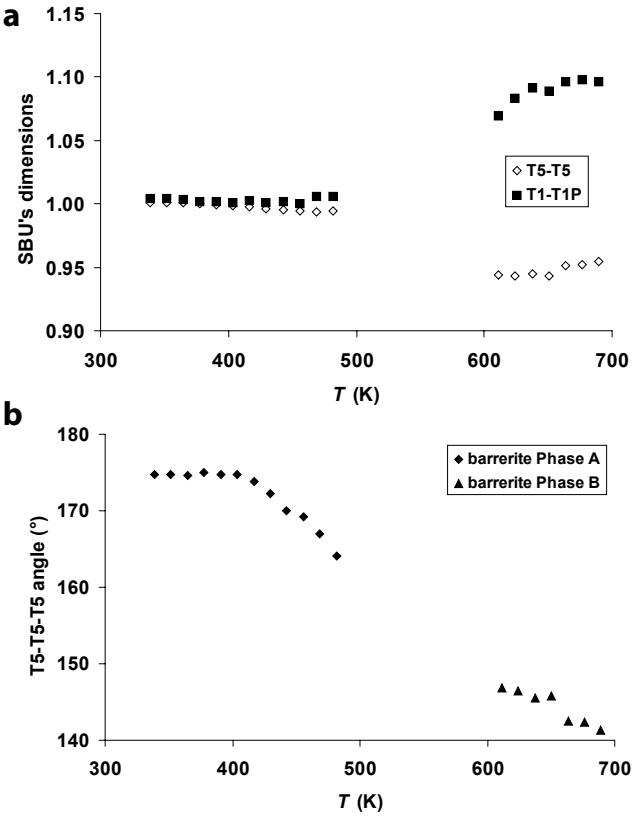

FIGURE 6. (**a**) Variation of the $4^2 5^4$ SBU dimensions (T5-T5 and T1-T1P distances) vs. temperature, as calculated from the structural refinements. (**b**) Plot of the T5-T5-T5 angle vs. temperature.

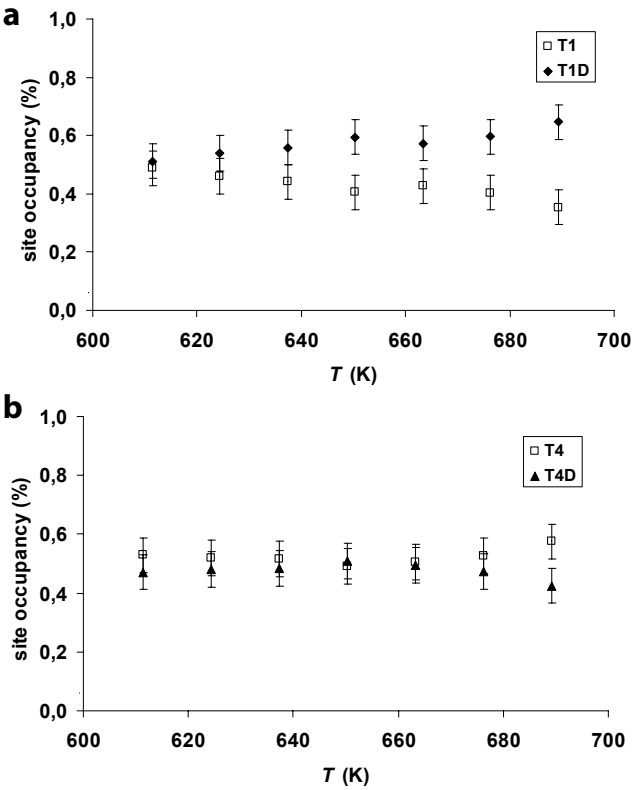

FIGURE 7. Refined occupancies of "face-sharing" tetrahedral sites (**a**) T1 and T1D and (**b**) T4 and T4D vs. temperature above 600 K.

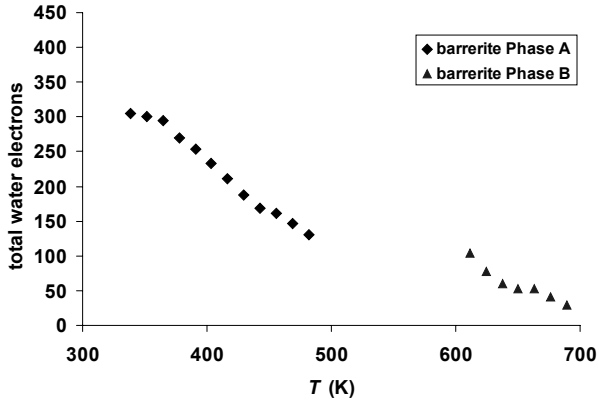

FIGURE 8. Total water content vs. temperature, calculated by subtracting from the total number of electrons, obtained by the occupancy factors of all the extraframework sites, the number of electrons corresponding to the cations, assumed constant during the whole dehydration process.

further factor was probably fundamental, i.e., the dehydration in vacuum (ex situ experiment) or in air (in situ experiment). This extrinsic factor in the dehydration process of barrerite was not relevant because both the in situ and ex situ experiments were performed in air.

ACKNOWLEDGMENTS

Two anonymous reviewers are kindly acknowledged for their suggestions. The European Synchrotron Radiation Facility is kindly acknowledged for allocation of beam-time under proposal CH545.

REFERENCES CITED

Ackermann, R.S. and Sorrell, C.A. (1974) Thermal expansion and the high-low transformation in quartz, I high-temperature X-ray studies. Journal of Applied Crystallography, 7, 431–437.

Alberti, A. (1972) On the crystal structure of the zeolite heulandite. Tschermaks Mineralogische Petrographische Mitteilungen, 18, 129–146.

——— (1973) The structure type of heulandite B (Heat-collapsed phase). Tschermaks Mineralogische Petrographische Mitteilungen, 19, 173–184.

Alberti, A. and Martucci A. (2005) Phase transformations and structural modifications induced by heating in microporous materials. Studies in Surface Science and Catalysis, 155, 19–43.

Alberti, A. and Vezzalini, G. (1978) Crystal structures of heat-collapsed phases of barrerite. In L.B. Sand and J. Mumpton, Eds., Natural Zeolites. Occurrence, Properties, Use, p. 85–98. Pergamon Press, New York.

——— (1983) The thermal behavior of heulandites: Structural study of the dehydration of Nadap heulandite. Tschermaks Mineralogische Petrographische Mitteilungen, 31, 259–270.

——— (1984) Topological changes in dehydrated zeolites: Breaking of T-O-T oxygen bridges. In D. Olson and A. Bisio, Eds., Proceedings of the 6th International Zeolite Conference, Reno, 834–841. Butterworth, Guildford, U.K.

Alberti, A., Rinaldi, R., and Vezzalini, G. (1978) Dynamics of dehydration in stilbite-type structures: Stellerite Phase B. Physics and Chemistry of Minerals, 2, 365–375.

Alberti, A., Cariati, F., Erre, L., Piu, P., and Vezzalini, G. (1983) Spectroscopic investigation on the presence of OH in natural barrerite and in its collapsed phases. Physics and Chemistry of Minerals, 9, 189–191.

Alberti, A., Vezzalini, G., Cariati, F., Erre, L., and Piu, P. (1985) Dehydration and re-hydration of the zeolites with 4-4-1 SBUs: near i.r. evidence for topological changes in heulandite I. Zeolites, 5, 289–291.

Alberti, A., Sacerdoti, M., Quartieri, S., and Vezzalini, G. (1999) Heating-induced phase transformation in zeolite brewsterite: New 4- and 5-coordinated (Si,Al) sites. Physics and Chemistry of Minerals, 26, 181–186.

Alberti, A., Vezzalini, G., Quartieri, S., Cruciani, G., and Bordiga, S. (2001) Rehydration mechanisms in zeolites: Reversibility of the TOT breaking and tetrahedral cation migration in brewsterite. Microporous and Mesoporous Materials, 42, 277–287.

Arletti, R., Mazzucato, E., and Vezzalini, G. (2006) Influence of dehydration kinetics on T-O-T bridge breaking in zeolites with framework type STI: The case of stellerite. American Mineralogist, 91, 628–634.

Armbruster, T. (1993) Dehydration mechanism of clinoptilolite and heulandite: Single-crystal X-ray study of Na-poor, Ca-, K-, Mg-rich clinoptilolite at 100 K. American Mineralogist, 78, 260–264.

Armbruster, T. and Gunter, M.E. (1991) Stepwise dehydration of heulandite-clinoptilolite from Succor Creek, Oregon, U.S.A.: A single-crystal X-ray study at 100 K. American Mineralogist, 76, 1872–1883.

Baerlocher, Ch., Meier, W.M., and Olson, D.H. (2001) Atlas of zeolite framework types. Elsevier, Amsterdam.

Bish, D.L. and Carey, J.W. (2001) Thermal behavior of natural zeolites. In D.L. Bish and D.W. Ming, Eds., Natural Zeolites: Occurrence, Properties, Applications, 45, p. 403–452. Reviews in Mineralogy and Geochemistry, Mineralogical Society of America, Chantilly, Virginia.

Cromer, D.T. and Waber, J.R. (1974) Atomic scattering factors for X-rays. In J.A. Ibers and W.C. Hamilton, Eds., International Tables for X-Ray Crystallography, Vol. IV, Section 2.2, p. 99–101. The Kynoch Press, Birmingham, U.K.

Cruciani, G. (2006) Zeolites upon heating: Factors governing their thermal stability and structural changes. Journal of Physics and Chemistry of Solids, 67, 1973–1994.

Cruciani, G., Artioli, G., Gualtieri, A., Stahl, K., and Hanson, J.C. (1997) Dehydration dynamics of stilbite using synchrotron X-ray powder diffraction. American Mineralogist, 82, 729–739.

Di Renzo, F. and Gabelica, Z. (1997) Barrerite and other zeolites from Kuiu and Kupreanof islands, Alaska. Canadian Mineralogist, 35, 691–698.

Donnay, G., Wyart, J., and Sabatier, G. (1959) Structural mechanism of thermal and compositional transformations in silicates. Zeitschrift für Kristallographie, 112, 161–168.

Galli, E. (1971) Refinement of the crystal structure of stilbite. Acta Crystallographica, B27, 833–841.

Galli, E. and Alberti, A. (1975a) The crystal structure of stellerite. Bulletin de la Société Francoise de Minéralogie et de Cristallographie, 98, 11–18.

——— (1975b) The crystal structure of barrerite. Bulletin de la Société Francoise de Minéralogie et de Cristallographie, 98, 331–340.

Larson, A.C. and Von Dreele, R.B. (2000) General structure analysis system (GSAS). Los Alamos National Laboratory, New Mexico, Report LAUR 86-748.

Meneghini, C., Artioli, G., Balerna, A., Gualtieri, A.F., Norby, P., and Mobilio, S. (2001) Multipurpose imaging-plate camera for in situ powder XRD at the GILDA beamline. Journal of Synchrotron Radiation, 8, 1162–1166.

Merkle, A.B. and Slaughter, M. (1968) Determination and refinement of the structure of heulandite. American Mineralogist, 53, 1120–1138.

Miller, S.A. and Taylor, J.C. (1985) Neutron single crystal diffraction study of an Australian stellerite. Zeolites, 5(1), 7–10.

Mortier, W.J. (1983) Thermal stability of the stilbite-type framework: crystal structure of the dehydrated sodium/ammonium exchange form. American Mineralogist, 68, 414–419.

Norby, P. (1997) Synchrotron powder diffraction using imaging plates: crystal structure determination and Rietveld refinement. Journal of Applied Crystallography, 30, 21–30.

Passaglia, E. and Pongiluppi, D. (1974) Sodian stellerite from Capo Pula, Sardegna. Lithos, 7, 69–73.

——— (1975) Barrerite, a new natural zeolite. Mineralogical Magazine, 40, 208.

Passaglia, E. and Sacerdoti, M. (1982) Crystal structural refinement of Na-exchanged stellerite. Bulletin de Minéralogie, 105, 338–442.

Passaglia, E., Galli, E., Leoni, L., and Rossi, G. (1978) The crystal chemistry of stilbites and stellerites. Bulletin de Minéralogie, 101, 368–375.

Pearce, J.R., Mortier, W.J., King, G.S.D., Pluth, J.J., Steele, I.M., and Smith, J.V. (1980) Stabilization of the stilbite-type framework: Crystal structure of the dehydrated NH4-exchanged form. In L.V.C. Rees, Ed., Proceedings of the Fifth International Conference on Zeolites, p. 261–268. Naples, Heyden, London.

Sacerdoti, M. (2007) The crystal structure of zeolite barrerite dehydrated in air at 400–450 °C. Microporous and Mesoporous Materials, 102, 299–303.

Sacerdoti, M., Sani, A., and Vezzalini, G. (1999) Structural refinement of two barrerites from Alaska. Microporous and Mesoporous Materials, 30, 103–109.

Sacerdoti, M., Vezzalini, G., and Quartieri, S. (2000) Dehydration mechanism in brewsterite: single-crystal X-ray diffraction study. Microporous and Mesoporous Materials, 41, 107–118.

Slaughter, M. (1970) Crystal structure of stilbite. American Mineralogist, 55, 387–397.

Ståhl, K. and Hanson, J.C. (1999) Multiple cation sites in dehydrated brewsterite. An in situ X-ray synchrotron powder diffraction study. Microporous and Mesoporous Materials, 32, 147–158.

Toby, B.H. (2001) EXPGUI, a graphical user interface for GSAS. Journal of Applied Crystallography, 34, 210–213.

MANUSCRIPT RECEIVED DECEMBER 28, 2007
MANUSCRIPT ACCEPTED JULY 9, 2008
MANUSCRIPT HANDLED BY HONGWU XU